



Contents lists available at ScienceDirect

NeuroImage

journal homepage: www.elsevier.com/locate/ynimg

1 Randomized parcellation based inference

Q1 Benoit Da Mota^{a,b,*}, Virgile Fritsch^{a,b}, Gaël Varoquaux^{a,b}, Tobias Banaschewski^{e,f}, Gareth J. Barker^d,
 3 Arun L.W. Bokde^{j,k}, Uli Bromberg^g, Patricia Conrod^{d,h}, Jürgen Gallinatⁱ, Hugh Garavan^{j,s,t}, Jean-Luc Martinot^{l,m},
 4 Frauke Nees^{e,f}, Tomas Paus^{n,o,p}, Zdenka Pausova^r, Marcella Rietschel^{e,f}, Michael N. Smolka^q, Andreas Ströhleⁱ,
 5 Vincent Frouin^b, Jean-Baptiste Poline^{b,c}, Bertrand Thirion^{a,b,*}, the IMAGEN consortium²

6 ^a Parietal Team, INRIA Saclay-Île-de-France, Saclay, France

7 ^b CEA, DSV, I2BM, Neurospin bât 145, 91191 Gif-Sur-Yvette, France

8 ^c Henry H. Wheeler Jr. Brain Imaging Center, University of California at Berkeley, USA

9 ^d Institute of Psychiatry, Kings College London, UK

10 ^e Central Institute of Mental Health, Mannheim, Germany

11 ^f Medical Faculty Mannheim, University of Heidelberg, Germany

12 ^g Universitätsklinikum Hamburg Eppendorf, Hamburg, Germany

13 ^h Department of Psychiatry, Université de Montréal, CHU Ste. Justine Hospital, Canada

14 ⁱ Department of Psychiatry and Psychotherapy, Campus Charité Mitte, Charité Universitätsmedizin Berlin, Germany

Q4 Q3 ^j Institute of Neuroscience, School of Medicine, Trinity College Dublin, Dublin, Ireland

16 ^k Discipline of Psychiatry, School of Medicine, Trinity College Dublin, Dublin, Ireland

17 ^l Institut National de la Santé et de la Recherche Médicale, INSERM CEA Unit 1000 "Imaging & Psychiatry", University Paris Sud, Orsay, Maison de Solenn, University Paris Descartes, Paris, France

18 ^m AP-HP Department of Adolescent Psychopathology and Medicine, Maison de Solenn, University Paris Descartes, Paris, France

19 ⁿ Rotman Research Institute, University of Toronto, Toronto, Canada

20 ^o School of Psychology, University of Nottingham, UK

21 ^p Montreal Neurological Institute, McGill University, Canada

22 ^q Neuroimaging Center, Department of Psychiatry and Psychotherapy, Technische Universität Dresden, Germany

23 ^r The Hospital for Sick Children, University of Toronto, Toronto, Canada

24 ^s Department of Psychiatry, University of Vermont, USA

25 ^t Department of Psychology, University of Vermont, USA

ARTICLE INFO

Article history:

28 Accepted 5 November 2013

29 Available online xxxx

Keywords:

34 Group analysis

35 Parcellation

36 Reproducibility

37 Multiple comparisons

38 Permutations

ABSTRACT

Neuroimaging group analyses are used to relate inter-subject signal differences observed in brain imaging with behavioral or genetic variables and to assess risks factors of brain diseases. The lack of stability and of sensitivity of current voxel-based analysis schemes may however lead to non-reproducible results. We introduce a new approach to overcome the limitations of standard methods, in which active voxels are detected according to a consensus on several random parcellations of the brain images, while a permutation test controls the false positive risk. Both on synthetic and real data, this approach shows higher sensitivity, better accuracy and higher reproducibility than state-of-the-art methods. In a neuroimaging–genetic application, we find that it succeeds in detecting a significant association between a genetic variant next to the *COMT* gene and the BOLD signal in the left thalamus for a functional Magnetic Resonance Imaging contrast associated with incorrect responses of the subjects from a *Stop Signal Task* protocol.

© 2013 Elsevier Inc. All rights reserved.

Introduction

Analysis of brain images acquired on a group of subjects makes it possible to draw inferences on regionally-specific anatomical properties

of the brain, or its functional organization. The major difficulty with such studies lies in the inter-subject variability of brain shape and vasculature. In functional studies, a task-related variability of subject performance is also observed. The standard-analytic approach is to register and normalize the data in a common reference space. However a perfect voxel-to-voxel correspondence cannot be attained, and the impact of anatomical variability is tentatively reduced by smoothing (Frackowiak et al., 2003). This problem holds for any statistical test, including those associated with multivariate procedures. In the absence of ground truth, choosing the best procedure to analyze the data is a challenging problem. Practitioners as well as methodologists tend to prefer

* Corresponding authors at: CEA, DSV, I2BM, Neurospin bât 145, 91191 Gif-Sur-Yvette, France.

E-mail addresses: benoit.da_mota@inria.fr (B. Da Mota), bertrand.thirion@inria.fr (B. Thirion).

¹ These authors contributed equally to this work.

² URL: <http://www.imagen-europe.com>

1053-8119/\$ – see front matter © 2013 Elsevier Inc. All rights reserved.

<http://dx.doi.org/10.1016/j.neuroimage.2013.11.012>

Please cite this article as: Da Mota, B., et al., Randomized parcellation based inference, NeuroImage (2013), <http://dx.doi.org/10.1016/j.neuroimage.2013.11.012>

models that maximize the sensitivity of a test under a given control for false detections. The level of sensitivity conditional to this control is indeed informative on the usefulness of a model.

Classic statistical tests for neuroimaging

The reference approach in neuroimaging is to fit and test a model at each voxel (univariate voxelwise method), but the large number of tests performed yields a multiple comparison problem. The statistical significance of the voxel intensity test can be corrected with various statistical procedures. First, Bonferroni correction consists in adjusting the significance threshold by dividing it by the number of tests performed. This approach is known to be conservative, especially when non-independent tests are involved, which is the case of neighboring voxels in neuroimaging. Another approach consists in a permutation test to perform a family-wise correction of the p-values (Nichols and Holmes, 2002). Although computationally costly, this method has been shown to yield more sensitive results than studies involving Bonferroni-corrected experiments (Pettersson et al., 1999). A good compromise between computation cost and sensitivity can be found in analytic corrections based on Random Field Theory (RFT), in which the smoothness of the images is estimated (Worsley et al., 1992). However, this approach requires both high threshold and data smoothness to be really effective (Hayasaka et al., 2004).

Another widely used method is a test on cluster size, which aims to detect spatially extended effects (Friston et al., 1993; Poline and Mazoyer, 1993; Roland et al., 1993). The statistical significance of the size of an activation cluster can be obtained with theoretical corrections based on the RFT (Hayasaka et al., 2004; Worsley et al., 1996b) or with a permutation test (Holmes et al., 1996; Nichols and Holmes, 2002). Cluster-size tests tend to be more sensitive than voxel-intensity tests, especially when the signal is spatially extended (Friston et al., 1996; Moorhead et al., 2005; Poline et al., 1997), at the expense of a strong statistical control on all the voxels within such clusters. This approach however suffers from several drawbacks. First, such a procedure is intrinsically unstable and its result depends strongly on an arbitrary cluster-forming threshold (Friston et al., 1996). The threshold-free cluster enhancement (TFCE) addresses this issue, by avoiding the choice of an explicit, fixed threshold (Salimi-Khorshidi et al., 2011; Smith and Nichols, 2009) but leads to other arbitrary choices: the TFCE statistic mixes cluster-extent and cluster-intensity measures in proportions that can be defined by the user. More generally, tests that combine cluster size and voxel intensity have been proposed (Hayasaka and Nichols, 2004; Poline et al., 1997). Second, the correlation between neighboring voxels varies across brain images, which makes detection difficult where the local smoothness is low. Combining permutations and RFT to adjust for spatially-varying smoothness leads to more sensitive procedures (Hayasaka et al., 2004; Salimi-Khorshidi et al., 2011). A more complete discussion of the limitations and comparisons of these techniques can be found in (Moorhead et al., 2005; Pettersson et al., 1999).

Spatial models for group analysis in neuroimaging

Spatial models try to overcome the lack of correspondence between individual images at the voxel level. The most straightforward and widely used technique consists of smoothing the data to increase the overlap between subject-specific activated regions (Worsley et al., 1996a). In the literature, several approaches propose more elaborate techniques to model the noise in neuroimaging, like Markov Random Fields (Ou et al., 2010), wavelet decomposition (Ville et al., 2004), spatial decomposition or topographic methods (Flandin and Penny, 2007; Friston and Penny, 2003) and anatomically informed models (Keller et al., 2009). These techniques are not widely used probably because they are computationally costly and not always well-suited for analysis of a group of subjects. A popular approach consists of working with

subject-specific Regions of Interest (ROIs), that can be defined in a way that accommodates inter-subject variability (Nieto-Castanon et al., 2003). The main limitation of such an approach (Bohland et al., 2009) is that there is no widely accepted standard for partitioning the brain, especially for the neocortex. Data-driven parcellation was proposed by Thirion et al. (2006) to overcome this limitation: they improve the sensitivity of random effect analysis by considering parcels defined at the group level.

Neuroimaging–genetic studies

While most studies investigate the difference of activity between groups or the level of activity within a population, neuroimaging studies are often concerned by testing the effect of exogeneous variables on imaging target variables, and there is increasing interest in the joint study of neuroimaging and genetics to improve understanding of both normal and pathological variability of the brain organization. Single nucleotide polymorphisms (SNPs) are the most common genetic variants used in such studies: They are numerous and represent approximately 90% of the genetic between-subject variability (Collins et al., 1998). Voxel intensity and cluster size methods have been used for genome-wide association studies (GWAS) (Stein et al., 2010), but the multiple comparison problem does not permit finding significant results, despite efforts to estimate the effective number of tests (Gao et al., 2010) or by running computationally expensive, but accurate permutation tests (Da Mota et al., 2012). Recently, important efforts have been done to design more sophisticated multivariate methods (Floch et al., 2012; Kohannim et al., 2011; Vounou et al., 2010), the results of which are more difficult to interpret; another alternative is to work at the gene level instead of SNPs (Ge et al., 2012; Hibar et al., 2011).

The randomized parcellation approach

The parcellation model (Thirion et al., 2006) has several advantages: (i) it is a simple and easily interpretable method, (ii) by reducing the number of descriptors, it reduces the multiple comparisons problem, and (iii) the choice of the parcellation algorithm can lead to parcels adapted to the local smoothness. But parcellations, when considered as spatial functions, highly depend on the data used to construct them and the choice of the number of parcels. In general, a parcellation defined in a given context might not be a good descriptor in a slightly different context, or may generalize poorly to new subjects. This implies a lack of reproducibility of the results across subgroups, as illustrated later in Fig. 7. The weakness of this approach is the large impact of a parcellation scheme that cannot be optimized easily for the sake of statistical inference; it may thus fail to detect effects in poorly segmented regions. We propose to solve this issue by using several randomized parcellations (Bühlmann et al., 2012; Varoquaux et al., 2012) generated using resampling methods (bootstrap) and average the corresponding statistical decisions. Replacing an estimator such as parcel-level inference by means of bootstrap estimates is known to stabilize it; a fortunate consequence is that the reproducibility of the results (across subgroups of subjects) is improved. Formally, this can be understood as handling the parcellation as a hidden variable that needs to be integrated out in order to obtain the posterior distribution of statistical values. The final decision is taken with regard to the stability of the detection of a voxel (Alexander and Lange, 2011; Meinshausen and Bühlmann, 2010) across parcellations, compared to the null hypothesis distribution obtained by a permutation test.

A multivariate problem: the detection of outliers

The benefits of the randomized parcellation approach can also be observed in multivariate analysis procedures, such as predictive modeling (Varoquaux et al., 2012) or outlier detection. In this work, we focus on

the latter: neuroimaging datasets often contain atypical observations; such *outliers* can result from acquisition-related issues (Hutton et al., 2002), bad image processing (Wu et al., 1997), or they can merely be extreme examples of the high variability observed in the population. Because of the high dimensionality of neuroimaging data, screening the data is very time consuming, and becomes prohibitive with large cohort studies. Covariance-based outlier detection methods have been proposed to perform statistically-controlled inclusion of subjects in neuroimaging studies (Fritsch et al., 2012) and yield a good detection accuracy. These methods rely on prior reduction of the data dimension which is obtained by taking signal averages within predefined brain parcels. As a consequence, the results depend on a fixed brain parcellation and are unstable. Randomization might thus improve the procedure.

Outline

In “Materials and methods”, we introduce methodological prerequisites and we describe the randomized parcellation approach. In “Experiments”, we provide the description of the experiments used to assess the performances of our procedure. We evaluate our approach on simulations and on real fMRI data for the random effect analysis problem. Then, we illustrate the interest of the approach for neuroimaging–genetic studies, on a gene candidate (*COMT*) which is widely investigated in the context of brain diseases. Finally, we show that this technique is suitable for detecting outliers in neuroimaging data, thus extending the application scope of randomized parcellations to multivariate analysis procedures. In “Results”, we report the results of the experiments and finally we discuss different aspects and choices that can influence the method performance.

Materials and methods

Statistical modeling for group studies

Neuroimaging studies are often designed to test the effect of miscellaneous variables on imaging target variables. For a study involving n subjects, neuroscientists generally consider the following model:

$$Y = X\beta + \epsilon,$$

where Y is a $n \times p$ matrix representing the signal of n subjects described each by p descriptors (e.g. voxels or parcels of an fMRI contrast image) and X is the $n \times (q_1 + q_2)$ set of q_1 explanatory variables, a predefined linear combination of which is to be tested for a non-zero effect, and q_2 covariables that explain some portion of the signal but are not to be tested for an effect. β are the coefficients of the model to be estimated, and ϵ is some Gaussian noise. Variables in X can be of any type (genetic, artificial, behavioral, experimental...). A standard univariate analysis technique consists in fitting p Ordinary Least Square (OLS) regressions, one for each column of Y , as a target variable, and each time perform a non-zero significance test on the $c^T\beta$ quantity, where $c \in \mathbb{R}^{q_1+q_2}$ is the *contrast vector* that defines the linear combination of the variables to be tested. This test involves the estimated coefficients of the model $\hat{\beta}$ and the noise estimate $\hat{\sigma}$ to compute a standard t - or F -statistic.

Parcellation and Ward algorithm

In functional neuroimaging, brain atlases are often used to provide a low-dimensional representation of the data by considering signal averages within groups of voxels (regions of interest). If those groups of voxels do not overlap and every voxel belongs to one group, the term *parcel* is employed, and the atlas is called a *parcellation*. In this work, we restrict ourselves to working with parcellations, although our methodology could be applied to any kind of brain

partition (set of ROIs). We construct parcellations from the images that we work on, because this data-driven approach better takes into account the unknown spatial data structure. Following (Michel et al., 2012; Varoquaux et al., 2012), we use spatially-constrained Ward hierarchical clustering (Ward, 1963) to cluster the voxels in K parcels, yielding what we will refer to as a K -parcellation. This approach creates a hierarchy of parcels represented as a tree. The root of the tree is the unique parcel that gathers all the voxels, the leaves being the parcels with only one voxel. When merging two clusters, the Ward criterion chooses the cluster that produces a supra-cluster with minimal variance. Any cut of the tree corresponds to a unique parcellation. This algorithm has several advantages: (i) It captures well local correlations into spatial clusters, (ii) efficient implementations exist (Pedregosa et al., 2011), and (iii) obtained parcellations are invariant by permutation of the subjects and sign of the input data. A gives a formal description of Ward’s clustering algorithm. We also show some examples of parcellations and discuss the geometric properties of the parcels.

Randomized parcellation based inference

Randomized parcellation based inference (RPBI) performs several standard analyses based on different parcellations and aggregates the corresponding statistical decisions. Let \mathcal{P} be a finite set of parcellations, and V be the set of voxels under consideration. Given a voxel v and a parcellation P , the parcel-based thresholding function θ_t is defined as:

$$\theta_t(v, P) = \begin{cases} 1 & \text{if } F(\Phi_P(v)) > t \\ 0 & \text{otherwise} \end{cases} \quad (1)$$

where $\Phi_P : V \rightarrow P$ is a mapping function that associates each voxel with a parcel from the parcellation P ($\forall v \in P^{(i)}, \Phi_P(v) = P^{(i)}$). For a predefined test, F returns the F -statistic associated with the average signal of a given parcel (a t or other statistic is also possible). Finally, the aggregating statistic at a voxel v is given by the counting function C_t :

$$C_t(v, \mathcal{P}) = \sum_{P \in \mathcal{P}} \theta_t(v, P). \quad (2)$$

$C_t(v, \mathcal{P})$ represents the number of times the voxel v was part of a parcel associated with a statistical value larger than t across the folds of the analysis conducted on the set of parcellations \mathcal{P} . We set the parameter t to ensure a Bonferroni-corrected control at $p < 0.1^3$ in each of the parcel-level analyses. In practice, the results are weakly sensitive to mild variations of t . In order to assess the significance of the counting statistic at each voxel, we perform a permutation test, i.e. we tabulate the distribution of $C_t(v, \mathcal{P})$ under the null hypothesis that there is no significant correlation between the voxels’ mean signal and the target variable. Depending on the comparison to be performed, we switch labels (comparison between groups) or we swap signs (testing that the mean is non-zero). As a result, we get a voxel-wise p-value map similar to a standard group analysis map (see Fig. 1). We obtain family-wise error control by tabulating the maximal value across voxels in the permutation procedure. The θ_t function can be replaced by any function that is convex with respect to t . In particular, the natural choice $\theta_t(v, P) = F(\Phi_P(v))$ yields similar results (not shown in the paper) but its computation requires much more memory since the $v \rightarrow \theta_t(v, P)$ mapping and bootstrap averages are no longer sparse. An important prerequisite for our approach is to generate several parcellations that are different enough from each other to guarantee that the analysis

³ We determine this value empirically to obtain a well-behaved null distribution of the counting statistic. With 1 target and 1000 parcels, it corresponds to a raw p-value $< 10^{-4}$.

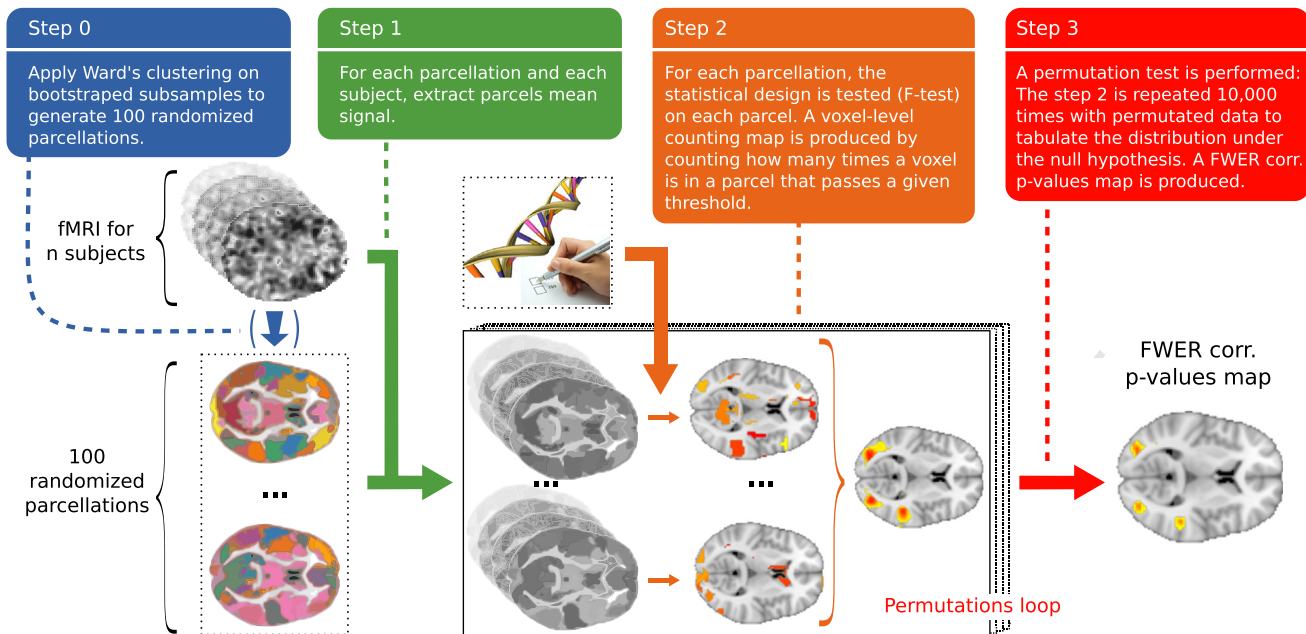


Fig. 1. Overview of the randomized parcellation based inference framework on an example with few parcels. The variability of the parcel definition is used to obtain voxel-level statistics.

301 conducted with each of those parcellations samples correctly the set of
 302 regions that display some activation for the effect considered. One way
 303 to achieve this is to take bootstrap samples of subjects and apply Ward's
 304 clustering algorithm to their contrast maps, to build brain parcellations
 305 that best summarize the data subsamples, i.e. so that the parcel-level
 306 mean signal summarizes the signal within each parcel, in each subject.
 307 If enough subjects are used, all the parcellations offer a good representation
 308 of the whole dataset. It is important that the bootstrap scheme
 309 generates parcellations with enough entropy (Varoquaux et al.,
 310 2012). Spatial models try to address the problem of imperfect voxel-
 311 to-voxel correspondence after coregistration of the subjects in the
 312 same reference space. Our approach is clearly related to anisotropic
 313 smoothing (Sol et al., 2001), in the sense that obtained parcels are
 314 not spherical and in the aggregation of the signals of voxels in a
 315 given parcel, certain directions are preferred. Unlike smoothing or spatial
 316 modeling applied as a preprocessing, our statistical inference embeds
 317 the spatial modeling in the analysis and decreases the number
 318 of tests and their dependencies. In addition to the expected increase
 319 of sensitivity, the randomization of the parcellations ensures a better
 320 reproducibility of the results, unlike inference on one fixed
 321 parcellation. Last, the $C_t(v, \mathcal{P})$ statistic is reliable in the sense that it
 322 does not depend on side effects such as the parcel size. This is formally
 323 checked in Appendix B.

324 Sensitivity and accuracy assessments

325 We want to assess the sensitivity of our approach at a fixed level of
 326 specificity and compare it to the other methods. Thus, we are interested
 327 in whether or not a significant effect was reported according to the different
 328 methods. Under the assumption that the method specificity is controlled
 329 with a given false positive rate, the method with the highest
 330 number of detections is the most sensitive.

331 Note that a direct comparison of the sensitivity of the different procedures
 332 (voxel-level, cluster-level, TFCE, parcel-based), i.e. their rate of
 333 detections, is not very meaningful. Indeed, only voxel-level statistics
 334 provide a strong control on false detections. The other procedures
 335 violate the subset pivotality condition, namely that the rejection of
 336 the null at a given location does not alter the distribution of the decision
 337 statistics under the null at other locations (see e.g. Westfall and

Troendle, 2008). This means that the rejection of the null at a given
 338 location is not independent of the rejection at the null at nearby
 339 locations; specifically, the rejection of the null at a given voxel is
 340 bound to the voxel in voxel-based tests, while it is not for other kinds
 341 of inferences considered here. Strictly speaking, those only reject a
 342 global null. Note however, that such a weak control on false detections
 343 is still useful in problems with small effect sizes (see "Neuroimaging-
 344 genetic study"). The ideal method would be able to detect small effects,
 345 but would be also quite specific about their location. That is why an
 346 analysis of the sensitivity should always be considered with an analysis
 347 of the accuracy.
 348

In our experiments, to estimate a method's accuracy, we construct
 349 Receiver Operating Characteristic (ROC) curves (Hanley and McNeil,
 350 1982) by reporting the proportion of true positives in the detections
 351 for different levels of false positives. The true/false positives are deter-
 352 mined according to a *ground truth* that is defined based on the simula-
 353 tion setup or empirically when dealing with real data. In practice, we
 354 are interested in low false positive rates, so we present the ROC curves
 355 in logarithmic scale.
 356

Use of randomized parcellation in multivariate models

357 Various neuroimaging methods rely on a prior dimension reduction
 358 of the data, and can therefore benefit from a randomized parcellation
 359 approach that stabilizes the ensuing statistical procedure. Beyond the
 360 specific case of group analysis investigated in this manuscript, we
 361 apply the randomized parcellation technique to the outlier detection
 362 task. Unlike group analysis, outlier detection can be formulated as a
 363 multivariate problem, especially because we consider covariance-
 364 based outlier detection (Fritsch et al., 2012), where an estimate of the
 365 data covariance matrix is computed and then used to provide an outlier
 366 score for each observation, i.e. correlations between features are taken
 367 into account in the final decision about whether or not an image should
 368 be considered an outlier.
 369

IMAGEN, a neuroimaging-genetic study

370 IMAGEN is a European multicentric study involving adolescents
 371 (Schumann et al., 2010). It contains a large functional neuroimaging
 372

373 database with fMRI associated with 99 different contrast images for
 374 4 protocols in more than 2000 subjects, who gave informed signed
 375 consent. Regarding the functional neuroimaging data, the faces pro-
 376 tocol (Grosbras and Paus, 2006) was used, with the [angry faces-
 377 control] contrast, i.e. the difference between watching angry faces
 378 and non-biological stimuli (concentric circles). We also use the
 379 Stop Signal Task protocol (Logan, 1994) (SST), with the activation
 380 during a [go wrong] event, i.e. when the subject pushes the wrong
 381 button. Images from the Modified Incentive Delay task (Knutson
 382 et al., 2000) (MID) were used to construct alternative randomized
 383 parcellations.

384 Eight different 3 T scanners from multiple manufacturers (GE,
 385 Siemens, Philips) were used to acquire the data. Standard preprocessing,
 386 including slice timing correction, spike and motion correction, temporal
 387 detrending (functional data), and spatial normalization (anatomical
 388 and functional data), were performed using the SPM8 software
 389 and its default parameters; functional images were resampled at
 390 3 mm resolution. All images were warped in the MNI152 coordinate
 391 space using a study-specific template. Obvious outliers detected using
 392 simple rules such as large registration or segmentation errors
 393 or very large motion parameters were removed after this step.
 394 BOLD time series was recorded using Echo-Planar Imaging, with
 395 TR = 2200 ms, TE = 30 ms, flip angle = 75° and spatial resolution
 396 3 mm × 3 mm × 3 mm. Gaussian smoothing at 5 mm-FWHM was fi-
 397 nally added.⁴ Contrasts were obtained using a standard linear model,
 398 based on the convolution of the time course of the experimental con-
 399 ditions with the canonical hemodynamic response function, together
 400 with standard high-pass filtering (period = 120 s) and temporally
 401 auto-regressive noise model. The estimation of the first-level was car-
 402 ried out using the SPM8 software. T1-weighted MPRAGE anatomical
 403 images were acquired with spatial resolution 1 mm × 1 mm × 1 mm,
 404 and gray matter probability maps were available for 1986 subjects as
 405 outputs of the SPM8 “New Segmentation” algorithm applied to the
 406 anatomical images. A mask of the gray matter was built by averaging
 407 and thresholding the individual gray matter probability maps. More
 408 details about data preprocessing can be found in (Thyreau et al.,
 409 2012). Genotyping was performed genome-wide using Illumina
 410 Quad 610 and 660 chips, yielding approximately 600,000 autosomic
 411 SNPs. 477,215 SNPs are common to the two chips and pass *plink* stan-
 412 dard parameters (Minor Allele Frequency > 0.05, Hardy-Weinberg
 413 Equilibrium $P < 0.001$, missing rate per SNP > 0.05).

414 Experiments

415 Random effect analysis on simulated data

416 We simulate fMRI contrast images as volumes of shape 40 × 40 ×
 417 40 voxels. Each contrast image contains a simulated 4 × 4 × 4 activa-
 418 tion patch at a given location, with a spatial jitter following a three-
 419 dimensional $N(0, I_3)$ distribution (coordinates of the jitter are rounded
 420 to the nearest integers). The strength of the activation is set so that
 421 the signal to noise ratio (SNR) peaks at 2 in the most associated
 422 voxel. The background noise is drawn from a (0,1) distribution,
 423 Gaussian-smoothed at σ_{noise} isotropic and normalized by its global
 424 empirical standard deviation. After superimposing noise and signal
 425 images, we optionally smooth at $\sigma_{\text{post}} = 2.12$ voxels isotropic, corre-
 426 sponding to a 5 voxel Full Width at Half Maximum (FWHM). Voxels
 427 with a probability above 0.1 to be active in a large sample test are
 428 considered as part of the ground truth. Ten subsamples (or groups)
 429 of 20 images are then generated to perform analyses. Each time,

RPBI was conducted with one hundred 1000-parcellations built from
 a bootstrapped selection of the 20 images involved. For each of the
 10 groups, we expect to obtain a p-value map that shows a significant
 effect at the mean location of generated artificial activations in the
 contrast images.

We investigate the ability of four methods to actually recover the
 region of activation:

- (i) voxel-level group analysis, which is the standard method in neuro-
 roimaging;
- (ii) cluster-size group analysis, which is known to be more sensitive
 than voxel-intensity group analysis;
- (iii) threshold-free cluster enhancement (TFCE) (Smith and Nichols,
 2009);
- (iv) RPBI, which is our contribution.

We control the specificity of each procedure by permutation testing.
 In order to ensure an accurate type 1 error control, we generate 400 sets
 of 20 images with no activation (i.e. the images are only noise with
 $\sigma_{\text{noise}} = 1$, and $\text{SNR} = 0$). We evaluate the false positive rate at
 voxel level for RPBI. We perform the same simulated data experiment
 with a more complex activation shape (shown in Fig. 2) as we think it
 better corresponds to activations encountered in real data. The rest of
 the experimental design remains the same and we perform the same
 comparison between methods.

454 Random effect analysis on real fMRI data

In this experiment, we work with an [angry faces-control] fMRI
 contrast. We kept data from 1430 subjects after removal of the
 subjects with missing data and/or bad or missing covariables. After
 standard preprocessing of the images, including registration of the
 subjects onto the same template, we test each voxel for a zero mean
 across the 1430 subjects with an OLS regression, including handed-
 ness and sex as covariables, yielding a reference voxel-wise p-value
 map. We threshold this map in order to keep 5% of the most active
 voxels (corresponding to $-\log_{10}P > 77.5$), and we consider it the
 ground truth. Since we use a voxel based threshold, the ground
 truth may be biased to voxel-level statistics (thus disadvantaging
 our method).

Our objective is to retrieve the population's reference activity
 pattern on subsamples of 20 randomly drawn subjects and compare
 the performance of several methods in this problem. Because of the re-
 duced number of subjects used, we cannot expect to retrieve the same
 activation map as in the full-sample analysis due to a loss in statistical

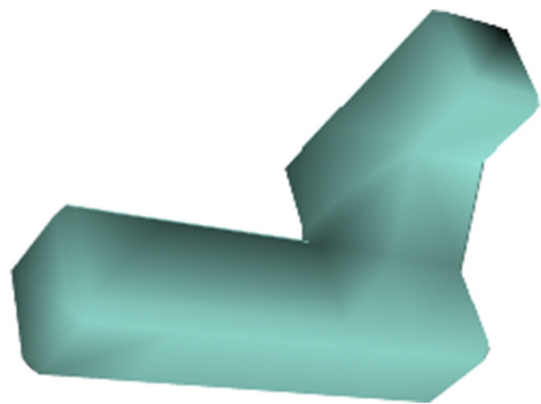


Fig. 2. Complex activation shape used for simulations. This activation shape is more scattered than a cube, and potentially better reflects the complex shape of real data activations. Note that, according to its original publication, TFCE performance is independent of the activation shape (Smith and Nichols, 2009).

⁴ Smoothing is applied only in the first-level analysis in order to improve the sensitivity of the General Linear Model that yields the contrast maps.

power. We therefore measure the sensitivity and we build ROC curves to assess the performance of the methods. We perform our experiment on 10 different subsamples and we use the same analysis methods as the previous experiment. We propose to observe the behavior of our method with the use of parcellations of different kinds. We perform analysis of the 10 different subsamples with the following parcellation schemes:

- (i) RPBI (sh. parcels) with parcellations built on bootstrapped subsamples of 150 images among the 1430 images corresponding to the fMRI contrast under study;
- (ii) RPBI (alt. parcels) with shared parcellations built on images corresponding to another, independent fMRI contrast;
- (iii) RPBI (rand. parcels) with shared parcellations built on smoothed Gaussian noise;

We also assess the stability of all these methods by counting how many times each voxel was associated to a significant effect across subsamples. We present the inverted cumulative normalized histogram of this count for each method, restricting our attention to the voxels that were reported at least once. A method is considered to be more stable than another if the same voxels appear more often, that is if its histogram shows many high values.

Neuroimaging–genetic study

The aim of this experiment is to show that RPBI has the potential to uncover new relationships between neuroimaging and genetics. We consider an fMRI contrast corresponding to events where subjects make motor response errors ([go wrong] fMRI contrast from a Stop Signal Task) and its associations with *Single-Nucleotide Polymorphisms* (SNPs) in the *COMT* gene. This gene codes for the Catechol-O-methyltransferase, an enzyme that catalyzes transfer of neurotransmitters like dopamine, epinephrine and norepinephrine, making it one of the most studied genes in relation to brain (Puls et al., 2009; Smolka et al., 2007). Subjects with too many missing voxels in the brain mask or with bad task performance were discarded. Regarding genetic variants, we kept 27 SNPs in the *COMT* gene (± 20 kb) that pass *plink* standard parameters (Minor Allele Frequency > 0.05 , Hardy–Weinberg Equilibrium $P > 0.001$, missing rate per SNP < 0.05). The ± 20 kb window includes some SNPs in the *ARVCF* gene, that are in *linkage disequilibrium* with SNPs in *COMT*. Age, sex, handedness and acquisition

center were included in the model as confounding variables. Remaining missing data were replaced by the median over the subjects for the corresponding variables. After applying all exclusion criteria 1372 subjects remained for analysis.

For each of the 27 SNPs, we perform a massively univariate voxel-wise analysis with the algorithm presented in (Da Mota et al., 2012), including cluster-size analysis (Hayasaka and Nichols, 2003), and RPBI through 100 different Ward's 1000-parcellations. To assess significance with a good degree of confidence we performed 10,000 permutations.

Outlier detection

We finally apply the concept of randomized parcellations to outlier detection. We work with a cohort of 1886 fMRI contrast images. In a first step, we randomly select 300 subjects and summarize the dataset by computing a 500-parcellation (obtained by Ward's) and averaging signal over each parcel. We perform a reference outlier detection on this dataset with a regularized version of a robust covariance estimator *RMCD-RP* (Fritsch et al., 2012). This outlier detection algorithm consists of fitting robust covariance estimators to random data projections. For the outlier detection we use the average of the Mahalanobis distances of the observations to the population mean in every projection subspace. In a second step, we perform outlier detections with *RMCD-RP* on random subsamples: We randomly draw a subsample of n subjects and perform 100 outlier detections with *RMCD-RP* on 100 different p -dimensional representations of the data defined by 100 Ward's p -parcellations built on 300 bootstrapped subjects from the whole cohort. Following the model of RPBI, we report how many times each subject was reported as an outlier through these 100 outlier detections and we use that number as an outlier score. We hence construct two Receiver Operating Characteristic (ROC) curves (Hanley and McNeil, 1982): one for randomized parcellation-based (RPB) outlier detection and the other as the average ROC curve of the 100 inner outlier detections used to obtain the RPB outlier detection. Finally, we report the rate of correct detections when 5% of false detections are accepted, to control the sensitivity of this test when wrongly rejecting few non-outlier data. These statistics make it possible to easily measure the accuracy improvement of RPB outlier detection across several experiments performed with different subsamples of n subjects (keeping the same reference decision obtained at the first step). In our experiment, we choose to work with

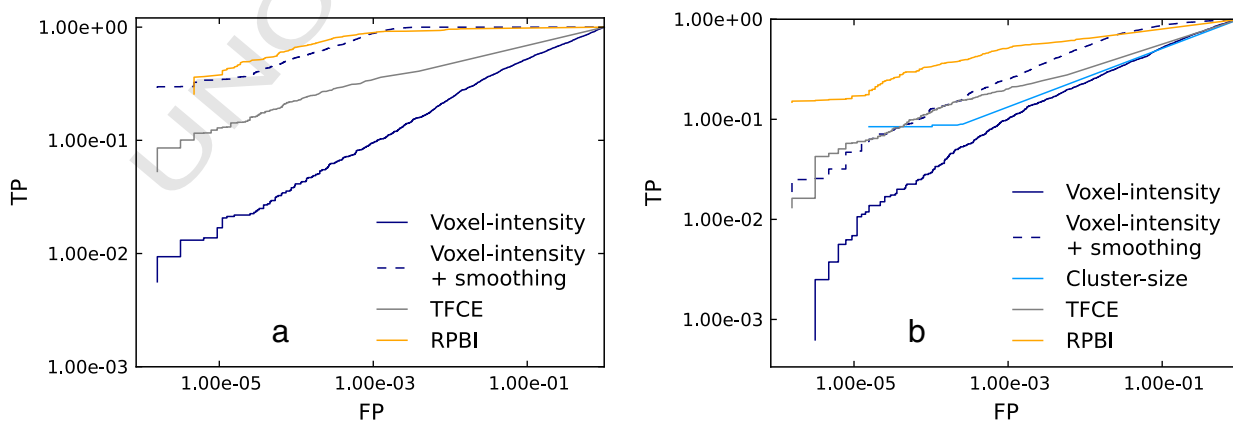


Fig. 3. Simulated data (cubic effect). ROC curves for various analysis methods across 10 random subsamples containing 20 subjects. SNR = 2 and noise spatial smoothness: (a) $\sigma_{\text{noise}} = 0$, (b) $\sigma_{\text{noise}} = 1$. The curves are obtained by thresholding the statistical brain maps at various levels, yielding as many points on the curves. The x-axis is the expected number of false positives per image. The curve for cluster-size inference could not be built for $\sigma_{\text{noise}} = 0$ because the detections correspond either to true positives only, or to false positives only. RPBI outperforms other methods.

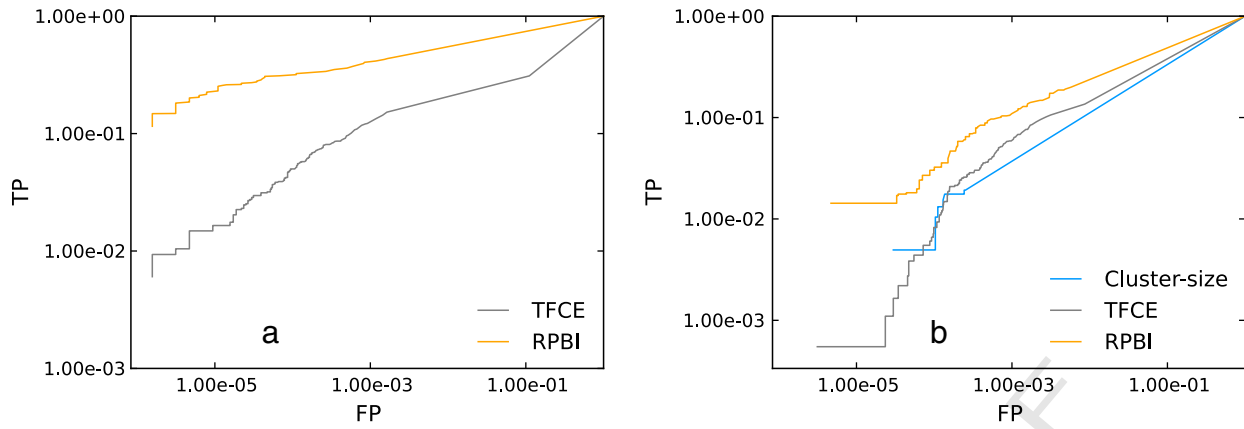


Fig. 4. Simulated data (complex activation shape). ROC curves for various analysis methods across 10 random subsamples containing 20 subjects, SNR = 2 and noise spatial smoothness: (a) $\sigma_{\text{noise}} = 0$, (b) $\sigma_{\text{noise}} = 1$. The curves are obtained by thresholding the statistical brain maps at various levels, yielding as many points on the curves. The x-axis is the expected number of false positives per image. The curve for cluster-size inference could not be built for $\sigma_{\text{noise}} = 0$ because the detections correspond either to true positives only, or to false positives only. For the same reason, voxel-intensity performance could not be presented in any of the plots. RPBI outperforms other methods.

551 $p = 100$ and $n = \{80,100,200,300,400\}$, yielding p/n configurations
 552 that correspond to various problem difficulties. For a fixed (n,p) couple,
 553 we run the experiment on 50 different subsamples and we present the
 554 rate of correct detections in a box-plot.

555 **Results**

556 *Random effect analysis on simulated data*

557 Voxel-intensity group analysis is the only method that benefits
 558 from a posteriori smoothing, while spatial methods lose sensitivity
 559 and accuracy when the images are smoothed. This is in agreement
 560 with the theory and the results of (Worsley et al., 1996a). Figs. 3
 561 and 4 show that detections made by spatial methods (cluster-size
 562 group analysis, TFCE and RPBI) do not come with wrongly reported
 563 effects in voxels close to the actual effect location. This would be
 564 the case for a method that simply extends a recovered effect to the neigh-
 565 boring voxels and would wrongly be thought to be more sensitive be-
 566 cause it points out more voxels. RPBI offers the best accuracy as its
 567 ROC curve dominates in Fig. 3. We could not always build ROC curves
 568 for the cluster-size method. This illustrates an issue of the cluster-
 569 forming threshold: most voxels do not pass the threshold and then

were discarded by the method, leading to a true positive rate equal 570
 to zero. The cluster-forming threshold directly acts on the recovery 571
 capability of the method, but lowering the threshold does not increase 572
 the sensitivity of this approach in general. By integrating over multi- 573
 ple thresholds, the TFCE partially addresses this issue. We also en- 574
 countered an issue in the construction of ROC curves for voxel- 575
 intensity based analysis in our simulations with a complex-shaped ac- 576
 tivation (see Fig. 4): either there were only true positives, or there 577
 were only false positives in our results, hence a lack of point for the 578
 construction of the ROC curves. When no signal is put in the data 579
 (SNR = 0), RPBI reports an activation 37 times over 400 at $P < 0.1$ 580
 FWER corrected, 20 times at $P < 0.05$ FWER corrected, and 4 times 581
 at $P < 0.01$ FWER corrected. In all cases, it corresponds to the nominal 582
 type I error rate. 583

584 *Random effect analysis on real fMRI data*

585 Fig. 5a shows the sensitivity improvement relative to cluster-size 586
 for various analysis methods under control for false detections at 587
 5% FWER. Cluster-size was taken as the reference because it is the 588
 method that yields the most sensitivity among state-of-the-art 589
 methods to which we compare RPBI to. RPBI achieves the best

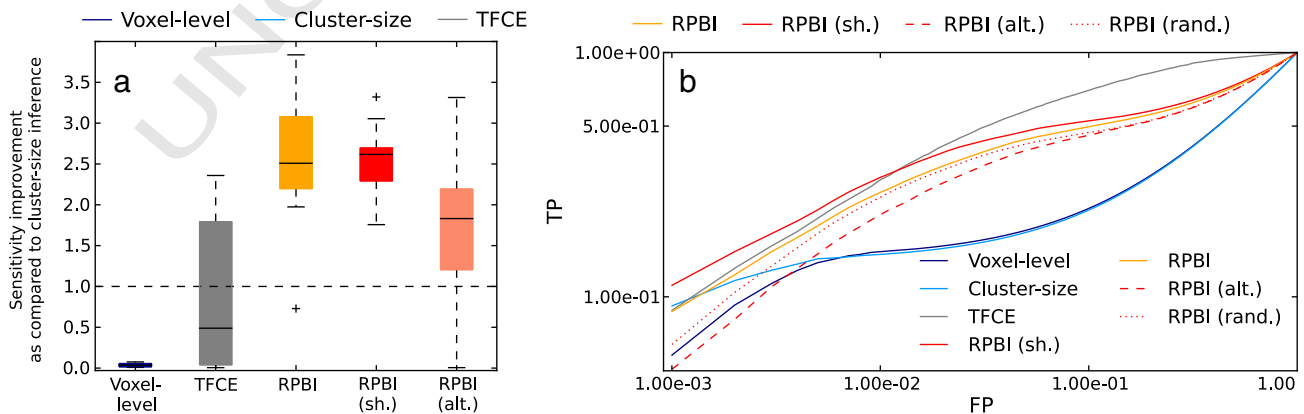


Fig. 5. Real fMRI data. Evaluation of the performances for various analysis methods across 10 random subsamples containing 20 subjects, on a [angry faces-control] fMRI contrast from the faces protocol. (a) Sensitivity improvement relative to cluster-size under control of the specificity at 5% FWER. (b) ROC curves built with a pseudo ground truth where 5% of the most active voxels across 1430 subjects are kept. RPBI and TFCE have similar performance for low false positive rates ($< 10^{-2}$), although TFCE performs slightly better.

590 sensitivity improvement, and RPBI with shared, alternative or random
 591 parcels are always more sensitive than TFCE. Voxel-level group analysis
 592 yields poor performance while cluster-size analysis is comparable
 593 to TFCE. These gains in sensitivity should be linked with a measure
 594 of accuracy (see “Materials and methods”). Fig. 5b shows the ROC
 595 curves associated with the performance of the methods under compar-
 596 ison. For acceptable levels of false positives ($<10^{-2}$), RPBI almost
 597 equals TFCE when we use parcellations that have been built on the
 598 contrast under study. RPBI with alternative or random parcels yields
 599 poor recovery although these approaches are based on the random-
 600 ized parcellation scheme. This demonstrates that the sensitivity is
 601 not a sufficient criterion and that the choice of parcellations plays
 602 an important role in the success of RPBI. Unlike simulations, real
 603 data may contain outliers, which reduce the effectiveness of all
 604 the presented methods. One benefit of RPBI with shared parcels is

605 that the impact of bad samples in the test set is lowered, because
 606 the parcellations are informed by potentially abundant side data.
 607 This requires other data from a similar protocol, but Fig. 5b shows
 608 that this approach outperforms other methods by finding more true
 609 positives.

610 The lack of stability of group studies is a well-known issue, yet it de-
 611 pends on the analysis performed (Strother et al., 2002; Thirion et al.,
 612 2007). RPBI has better reproducibility than the other methods, as
 613 shown in Fig. 7. The histogram of the RPBI method dominates, which
 614 means that significant effects were reported more often at the same lo-
 615 cation (i.e. the same voxel) across subgroups when using RPBI than
 616 when using the other methods. For RPBI with shared parcels, it is even
 617 more pronounced and this is explained by the fact that parcellations
 618 are shared across subgroups, which is another advantage to this
 619 method.

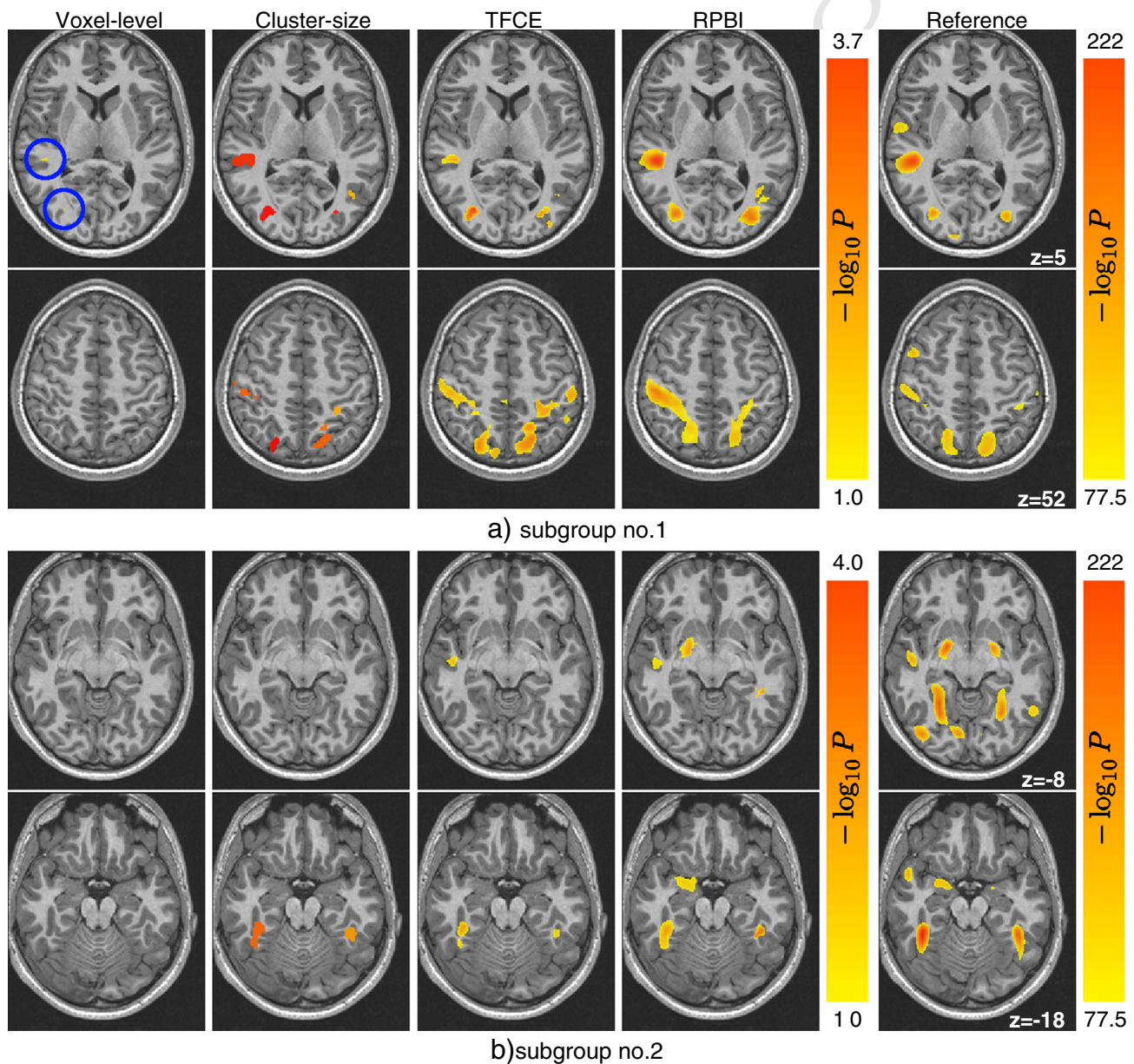


Fig. 6. Negative \log_{10} -value associated with a non-zero intercept test with confounds (handedness, site, sex), on a [angry faces–control] fMRI contrast from the faces protocol. The subgroups maps are thresholded at $-\log_{10}P > 1$ FWER corrected and the reference map at $-\log_{10}P > 77.5$ (i.e. 5% of the most active voxels). Small activation clusters are surrounded with a blue circle in order to make them visible.

620 In general, the same activation peaks rise from the cluster-size, the
 621 TFCE and the RPBI maps (see Fig. 6). The TFCE slightly improves the re-
 622 sults of cluster-size and provides voxel-level information. As can be seen
 623 in Fig. 6, the map returned by RPBI better matches the patterns of the
 624 reference map and is less scattered. Voxel-based group analysis clearly
 625 fails to detect some of the activation peaks.

626 Neuroimaging–genetic study

627 The SNP rs917478 yields the strongest correlation with the pheno-
 628 types and lies in an intronic region of ARVCF. The number of subjects
 629 in each genotype group is balanced: 523 homozygous with major
 630 allele, 663 heterozygous and 186 homozygous with minor allele. For
 631 RPBI, 31 voxels (resp. 81) are significantly associated with that SNP
 632 at $P < 0.05$ FWER corrected (resp. $P < 0.1$) in the left thalamus, a re-
 633 gion involved in sensory-motor cognitive tasks. The association peak
 634 has a p-value of 0.016 FWER corrected. Cluster-size inference finds
 635 this effect but with a higher p-value ($P = 0.046$). Voxel-based infer-
 636 ence does not find any significant effect. A significant association
 637 for rs917479 is reported only by RPBI; Fig. 8 shows that this SNP
 638 is in high linkage disequilibrium (LD) with rs917478 ($D' = 0.98$
 639 and $R^2 = 0.96$). As shown in Fig. 8, those SNPs are also in LD with
 640 rs9306235 and rs9332377 in *COMT*, the targeted gene for this study.
 641 Fig. 8 shows the thresholded p-value maps obtained with RPBI with
 642 rs917478.

643 The ARVCF gene has already been found to be associated with inter-
 644 mediate brain phenotypes and neurocognitive error tests in a study
 645 about schizophrenia (Sim et al., 2012). We applied our method on this
 646 gene, for which we have 33 SNPs, and did not find any effect except
 647 from rs917478 and SNPs in LD with it.

648 Outlier detection

649 Fig. 9 illustrates the accuracy of RPB outlier detection as com-
 650 pared to standard outlier detection performed on data issued from
 651 a single parcellation. We present the rate of correct detections
 652 when 5% false detections are accepted. Since the experiment is con-
 653 ducted on 50 subsamples of n subjects, we present the results
 654 for various values of n ($n \in \{80, 100, 200, 300, 400\}$) with box-plots.
 655 For a large number of subjects (low-dimensional settings: $n < p$)
 656 RPB outlier detection performs slightly better than standard outlier
 657 detection, while in high-dimensional settings ($p > n$) it clearly out-
 658 performs the classic approach. Relative results are the same when

659 allowing for any proportion of false detection comprising between
 660 0% and 10%.

661 Discussion

662 In this work, we introduce a new method for statistical inference
 663 on brain images (RPBI) based on a randomized version of the
 664 parcellation model (Thirion et al., 2006) that is stabilized by a boot-
 665 strap procedure. In both simulation and real data experiments, RPBI
 666 shows better performance (sensitivity, recovery and reproducibility)
 667 than standard methods. The strength of this method is that the deci-
 668 sion statistic takes into account the spatial structure of the data. Also,
 669 the randomization of the parcellations yields more reproducible
 670 results in view of between-subject variability and lowers the effect of
 671 inaccurate parcellation. Our experiments with simulated and real
 672 data show that the choice of the parcellations can greatly influence
 673 the success of RPBI. In this section, we discuss this choice. We also
 674 discuss some factors that can influence the method performance,
 675 such as images properties or tested features characteristics and com-
 676 putational aspects.

677 Brain parcellations

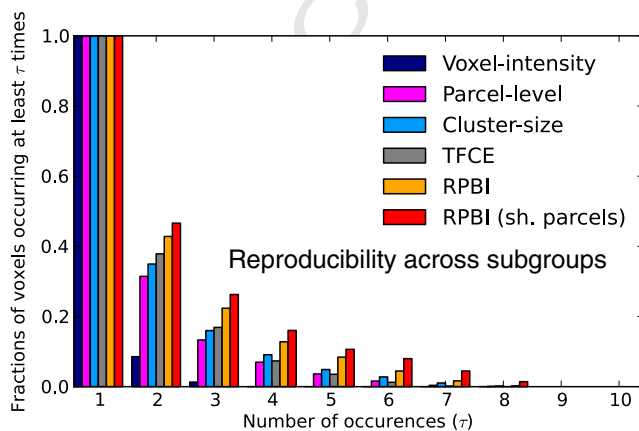
678 In our experiments, we used Ward clustering to build brain
 679 parcellations. The main advantage of this clustering algorithm is that
 680 it has the ability to take into account spatial pattern similarities be-
 681 tween a set of input images, which acts as a spatial regularization. In
 682 addition, the Ward criteria is designed such that, taking the mean sig-
 683 nal within each parcel as new features to describe one subject image
 684 gives the optimal data representation in terms of preserved informa-
 685 tion (for a fixed dimension corresponding to the number of parcels).
 686 Importantly, the variability of the parcellations is directly related to
 687 the variability and number of the images on which they are built. We
 688 determined empirically that using 1000 parcels is a good trade-off be-
 689 tween accurate parcellations and dimension reduction. This choice
 690 leads to using an average of 50 voxels per parcel, which is a good
 691 order of magnitude to describe the activation clusters. Note that, this
 692 number of parcels is far from standard brain atlases with, at best,
 693 a few hundred ROIs, suggesting that atlases are not well-suited for
 694 such studies. Our first real data experiment demonstrates that it is
 695 beneficial that the parcellations reflect the group spatial activity
 696 pattern of the fMRI contrast under study: when the parcellations are
 697 built on another fMRI contrast or on random noise, the final perfor-
 698 mance of persistence analysis drops back to the level of state-of-the-
 699 art methods in terms of accuracy.

700 RPBI and images properties

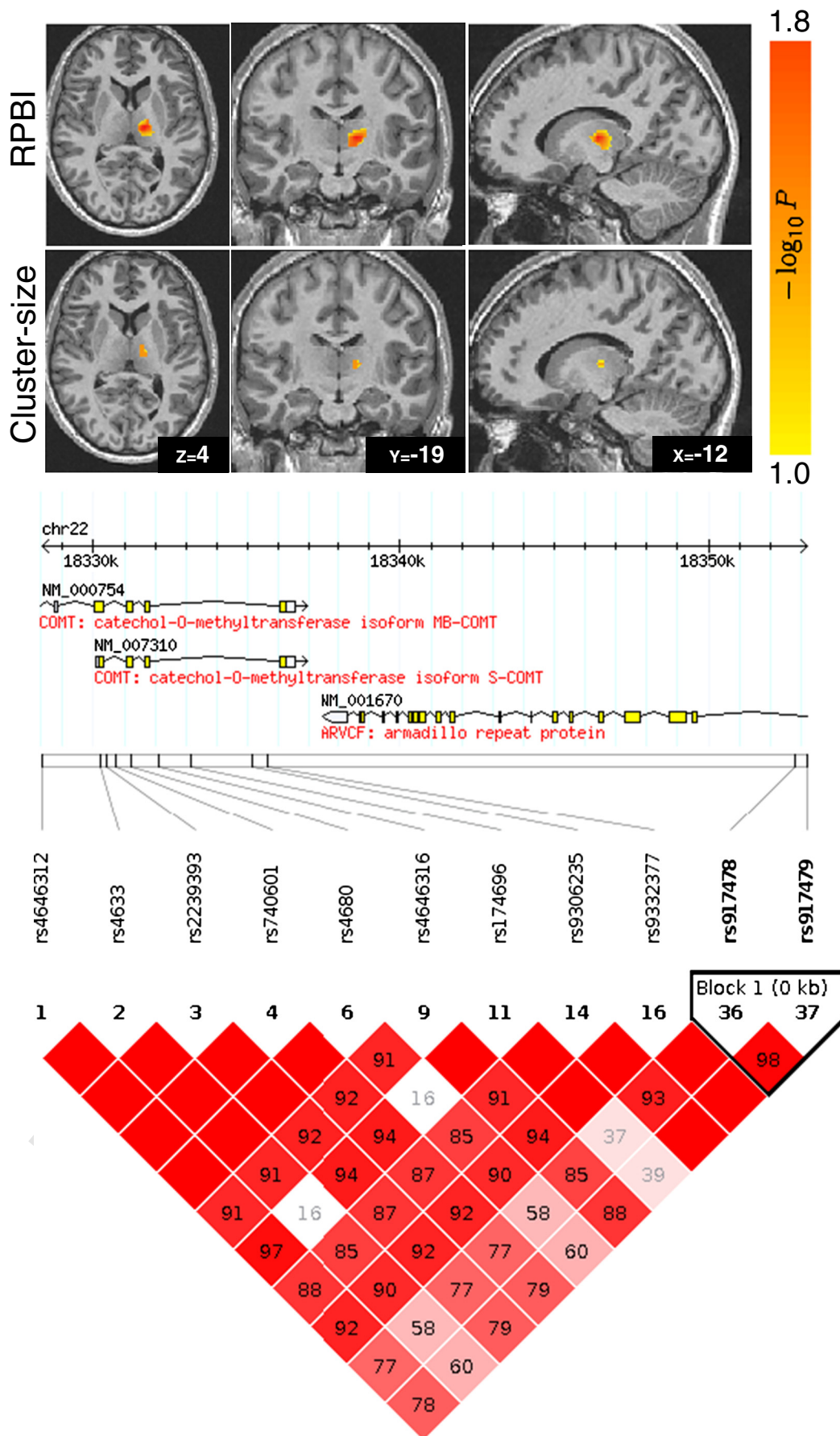
701 Our first experiment shows that RPBI performance drops when im-
 702 ages are smoothed a posteriori. Unlike voxel-intensity analysis,
 703 cluster-size analysis, TFCE and RPBI, which are spatial methods, suffer
 704 from data smoothing. In the presence of smooth noise, this experiment
 705 also shows that RPBI outperforms other methods. Our experiment on
 706 real data shows that RPBI can recover activations clusters of various
 707 size and shape, as visible on the effect maps reported in Fig. 6. Yet, the
 708 use of parcels clearly helps in focusing on activations with a spatial ex-
 709 tent of the order of the average parcel size. Cluster-size group analysis
 710 also focuses more easily on some activations with a given size, accord-
 711 ing to internal parameters such as the cluster forming threshold or an op-
 712 tional data smoothing. TFCE is designed to address this issue and clearly
 713 enhances the results of the cluster-size inference.

714 Sensitivity and reproducibility

715 Usually, the sensitivity of a procedure is compared under a given
 716 control for false positives. Under this criterion, RPBI outperforms



659 Fig. 7. Real fMRI data. Inverse cumulative histograms of the relative number of voxels that
 660 were reported as significant several times through the 10 subsamples ($P < 0.05$ FWER
 661 corrected), on a [angry faces–control] fMRI contrast from the faces protocol. Parcel-level in-
 662 ference yields results that are less reproducible than those of RPBI.



717 voxel-intensity, cluster-size analysis and TFCE (Fig. 5.a). By aggregating
 718 100×1000 measurements, RPBI drastically reduces the multiple compar-
 719 ison problem and stabilizes parcel-based statistics. Neuroimaging
 720 studies are subject to a lack of reproducibility and using the most sensi-
 721 tive procedure does not guarantee the unveiling of reproducible results
 722 (Strother et al., 2002; Thirion et al., 2007). Experiments on real data
 723 show the gain in terms of reproducibility of RPBI compared to other
 724 methods when the subset of subjects changes (Fig. 7). RPBI with shared
 725 parcels has a better recovery and yields more reproducible results
 726 across various analysis settings.

727 Randomized parcellation can be applied to various neuroimaging
 728 tasks. However, sensitivity improvement is not straightforward and
 729 may depend on problem-specific settings. In particular, our experiment
 730 about outlier detection suggests that multivariate statistical algorithms
 731 require a more subtle use of randomized parcellation in order to get sig-
 732 nificant sensitivity improvement.

733 Computational aspects

734 Our goal here is not to provide an exhaustive study of the computa-
 735 tional performance, but to report on our experience of the experiments
 736 performed. The procedure is separated into two distinct steps: (i) the
 737 generation of the 100 Ward K -parcellations and extraction of the signal
 738 means, then (ii) the statistical inference. The generation of parcellations
 739 is optional (parcellations can be replaced by precomputed ones), but
 740 Ward's hierarchical clustering algorithm is fast and this step takes
 741 only a few minutes on a desktop computer for 100 parcellations. The
 742 second step involves a permutation test. Our implementation fits a
 743 Massively Univariate Linear Model (Da Mota et al., 2012; Stein et al.,
 744 2010) in an optimized version adapted to permutation testing and our
 745 application. As a result, in our experiments with 20 subjects and
 746 10,000 permutations, the statistical inference takes only 1 min \times cores,
 747 i.e. 5 s on a 12-core computer. The total computation time thus amounts
 748 to a few minutes on a desktop computer and is limited by the construc-
 749 tion of the parcellations. Asymptotically, the computation time in-
 750 creases only linearly with the number of subjects and the number of
 751 variables to test, which is a desirable property to scale to larger prob-
 752 lems like neuroimaging-genetic studies.

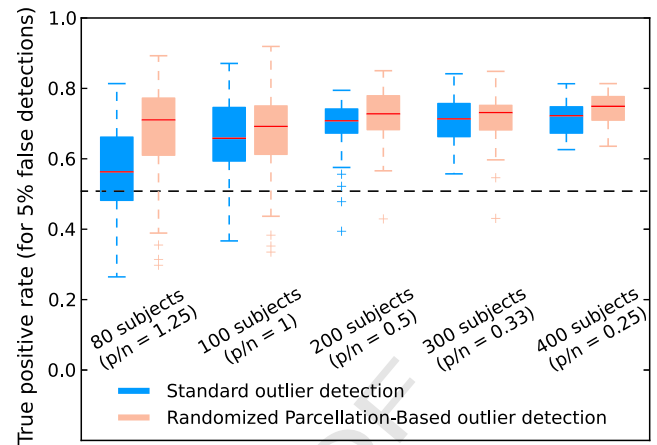
753 Conclusion

754 RPBI is a general detection method based on a consensus across
 755 bootstrap estimates that can be applied to various neuroimaging prob-
 756 lems such as group analyses or outlier detection. In our work, we use
 757 randomized parcellations to benefit from many ROI-based descriptions
 758 of our datasets that we construct with Ward's clustering. Simulations
 759 and real-data experiments show that RPBI is more sensitive and stable
 760 than state-of-the-art analysis methods. This is the case for various
 761 types of problems, including neuroimaging-genetic associations. We
 762 also demonstrate that the RPBI framework can be applied to outlier de-
 763 tection problem and improves detections accuracy.

764 Acknowledgments

765 This work was supported by Digiteo grants (HiDiNim project and
 766 ICoGeN project) and an ANR grant (ANR-10-BLAN-0128), as well the
 767 Microsoft INRIA joint center grant *A-brain*.

768 The data were acquired within the IMAGEN project, which received
 769 research funding from the E.U. Community's FP6, LSHM-CT-2007-



770 **Fig. 9.** Proportion of observations correctly tagged as outliers when 5% errors are accepted.
 771 Results are represented as boxes according to the number of subjects present in the sub-
 772 samples in which we seek outliers. Chance level is given by the dashed black line. RPBI
 773 outlier detection always outperforms standard outlier detection, although the difference
 774 between both is small and may not worth the implementation and computation costs. It
 775 is larger in the case where there are more features than subjects.

037286. This manuscript reflects only the authors' views and the Com- 770
 771 munity is not liable for any use that may be made of the information
 772 contained therein. 772

773 Appendix A. Formal description of Ward's clustering algorithm 773

774 Ward's clustering algorithm is a particular case of *hierarchical*
 775 *agglomerative clustering* (Johnson, 1967). Let $Y = \{y_1, \dots, y_p\} \in \mathbb{R}^{n \times p}$
 776 be a set of n fMRI volumes described by p voxels each. For two clusters
 777 of voxels c and c' , we define the distance: 777

$$\Delta(c, c') = \frac{|c||c'|}{|c| + |c'|} \|\langle Y \rangle_c - \langle Y \rangle_{c'}\|_2^2, \quad (\text{A.1})$$

778 where $\langle Y \rangle_c = \frac{1}{|c|} \sum_{j \in c} y^j$. For each partition $C = \{c_1, \dots, c_k\}$ of the set of 778
 779 voxels Y (i.e. $\cup_{c \in C} c = Y$ and $c_i \cap c_j = \emptyset \forall (c_i, c_j) \in C^2$), we note C^* the 780
 781 set of all pairs of clusters that share at least one neighboring voxel. 781
 782 Ward's clustering algorithm starts with an initial partition of p clusters 782
 783 $C = \{\{y_1\}, \dots, \{y_p\}\}$ that correspond to one singleton cluster per voxel. 783
 784 At each iteration, we merge the two clusters c_i and c_j of C^* that minimize 784
 785 the distance Δ : 785

$$(c_i, c_j) = \underset{(c, c') \in C^*}{\operatorname{argmin}} \Delta(c, c'). \quad (\text{A.2})$$

786 The spatial constraint comes from the fact that we restrict the 786
 787 solution of the minimization criterion to C^* . When constructing a 787
 788 K -parcellation, the algorithm stops when $\operatorname{card}(C) = K$. 788
 789

790 Fig. A.10 shows some example parcellations, while Fig. A.11 shows 790
 791 the size and compactness of the parcels. In "Materials and methods", 791
 792 we use various Ward's clustering scheme that simply correspond to 792
 793 different choices for Y . 793
 794

795 **Fig. 8.** Association study between 27 SNPs from the *COMT* gene (± 20 kb) and fMRI contrast phenotypes. Family wise corrected p-values map (thresholded at $P < 0.1$) obtained with RPBI (top row) and cluster-size inference (bottom row) for rs917478, the SNP with the strongest reported effect. Linkage disequilibrium reported by HapMap for SNPs with $MAF > 0.05$ in a European population (CEU + TSI). For the sake of readability, other SNPs in ARVCF are hidden. Red boxes without values correspond to maximum linkage disequilibrium, i.e. $D' = 1$. The found SNPs (rs917478 and rs917479) are in high linkage disequilibrium with two SNPs at the end of *COMT*, namely rs9306235 and rs9332377.

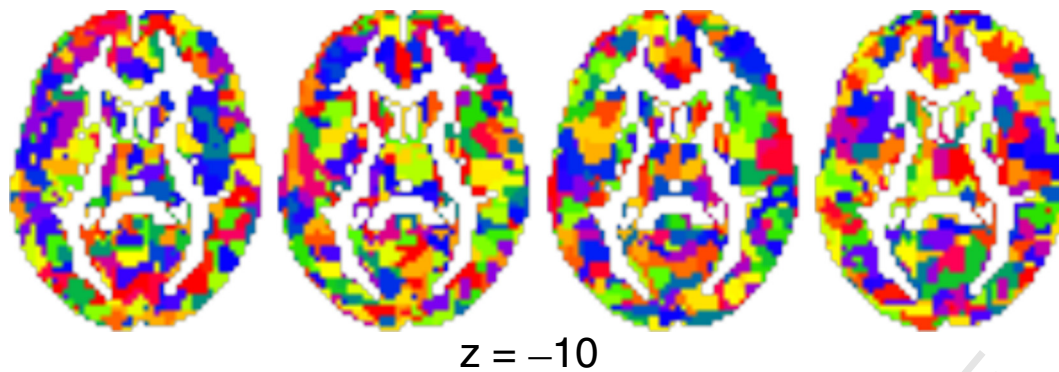


Fig. A.10. Example parcellations obtained with Ward's clustering algorithm. The [angry faces–control] fMRI contrast maps of 20 bootstrapped subjects were used.

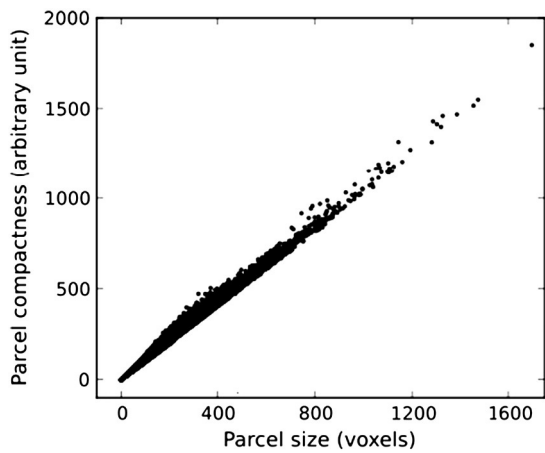


Fig. A.11. Size and compactness of the parcels obtained with Ward's clustering algorithm on fMRI contrast maps. For each parcel, the compactness is measured as the difference between a mask of the parcel and its 1-eroded image). One can observe a great variability in parcel size/compactness, which reflects the structure of the individual fMRI contrast maps.

Appendix B. Pivotality of the counting statistic

An important question is whether the counting statistic introduced in Eq. (1) is a valid statistic to detect activated voxels. One essential criterion for this is to check the pivotality, i.e. the convergence – under the null hypothesis – of the statistic distribution toward a law that is invariant under data distribution parameters. In the present case, the main deviation from pivotality could result from a distribution of (extreme) statistical values that depends on the parcel size: large parcels would represent fMRI signal averaged over larger domains, and thus would get typically lower values. This is indeed typically the case for the mean statistic (see Fig. B.12 (b)); however, we show for instance that the t statistic used in “Materials and methods” is very weakly influenced by the parcel size: we repeated the experiment described in “Materials and methods”, i.e. computing the t statistic on parcels obtained by Ward's algorithm, based on 100 random batches of 20 subjects, after permutation by random sign swap. We tabulate the t distribution according to the parcel size by using 10 size bins. The result, shown in Fig. B.12 (a), is that the effect, if any, is not detectable by visual inspection.

To test more precisely the independence on the t distribution with respect to the parcel size, we tested the equality of the mean, median and variance of the size-specific distributions using the One-way (mean), Kruskal (median), Bartlett (variance), Levene (variance) and Fligner (variance) tests as implemented in the SciPy library.⁵ All the tests are performed on the 10 bins jointly. We obtain the following p-values: One-way, $P = 0.36$; Kruskal, $P = 0.27$; Bartlett: $P = 0.95$;

Levene: $P = 0.016$; Fligner: $P = 0.06$. This means that there is only a small effect on the variance, as reported by the Levene test, that is more sensitive than Fligner (which is non-parametric) and Bartlett, which assumes Gaussian distributions. However this effect is very small, and has no obvious consequence on the number of peak values of the statistic; in particular, we do not observe monotonic trends with size. Note that the small effect fades out when using larger number of subjects (here, only $n = 20$ subjects per groups were used). Finally, we did not find any significant correlation between the number of detections above a given threshold (using uncorrected p-values of 10^{-2} , 10^{-3} , 10^{-4}) and the parcel size.

In conclusion, the effect of parcel size is too small to jeopardize the usefulness of the counting statistic.

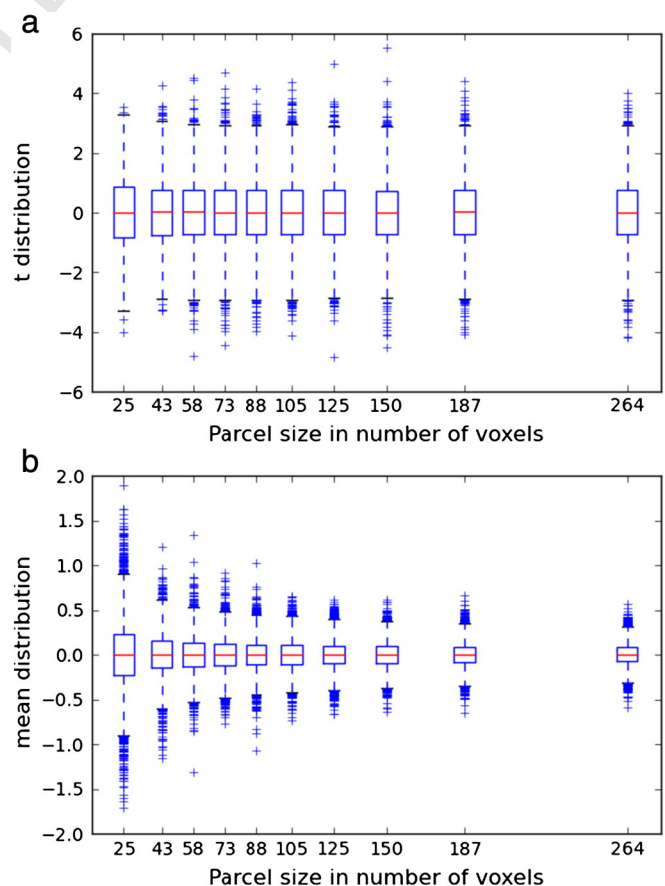


Fig. B.12. Impact of the parcel size on the distribution of the second-level one-sample t statistic (a) and of the mean value (b). While there is an obvious effect on the mean, there is no conspicuous effect on the t distribution.

⁵ <http://www.scipy.org/>.

833 **Appendix C. Supplementary data**

834 Supplementary data to this article can be found online at <http://dx.doi.org/10.1016/j.neuroimage.2013.11.012>.

836 **References**

- 837 Alexander, D.H., Lange, K., 2011. Stability selection for genome-wide association. *Genet. Epidemiol.* 35, 722–728.
- 838 Bohland, J.W., Bokil, H., Allen, C.B., Mitra, P.P., 2009. The brain atlas concordance problem: quantitative comparison of anatomical parcellations. *PLoS One* 4, e7200.
- 840 Bühlmann, P., Rütimann, P., van de Geer, S., Zhang, C.H., 2012. Correlated Variables in Regression: Clustering and Sparse Estimation (ArXiv e-prints).
- 842 Collins, F.S., Brooks, L.D., Chakravarti, A., 1998. A DNA polymorphism discovery resource for research on human genetic variation. *Genome Res.* 8, 1229–1231.
- 844 Da Mota, B., Frouin, V., Duchesnay, E., Laguitton, S., Varoquaux, G., Poline, J.B., Thirion, B., 2012. A fast computational framework for genome-wide association studies with neuroimaging data. 20th International Conference on Computational Statistics.
- 846 Flandin, G., Penny, W.D., 2007. Bayesian fMRI data analysis with sparse spatial basis function priors. *NeuroImage* 34, 1108–1125.
- 848 Floch, E.L., Guillemot, V., Frouin, V., Pinel, P., Lalanne, C., Trincherà, L., Tenenhaus, A., Moreno, A., Zilbovicius, M., Bourgeron, T., Dehaene, S., Thirion, B., Poline, J.B., Duchesnay, E., 2012. Significant correlation between a set of genetic polymorphisms and a functional brain network revealed by feature selection and sparse partial least squares. *NeuroImage* 63, 11–24.
- 854 Frackowiak, R., Friston, K., Frith, C., Dolan, R., Price, C., Zeki, S., Ashburner, J., Penny, W., 2003. *Human Brain Function*, second ed. Academic Press.
- 857 Friston, K.J., Penny, W., 2003. Posterior probability maps and spms. *NeuroImage* 19, 1240–1249.
- 858 Friston, K.J., Worsley, K.J., Frackowiak, R.S.J., Mazziotta, J.C., Evans, A.C., 1993. Assessing the significance of focal activations using their spatial extent. *Hum. Brain Mapp.* 1, 210–220.
- 862 Friston, K.J., Holmes, A., Poline, J.B., Price, C.J., Frith, C.D., 1996. Detecting activations in PET and fMRI: levels of inference and power. *NeuroImage* 4, 223–235.
- 864 Fritsch, V., Varoquaux, G., Thyreau, B., Poline, J.B., Thirion, B., 2012. Detecting outliers in high-dimensional neuroimaging datasets with robust covariance estimators. *Med. Image Anal.* 16, 1359–1370.
- 866 Gao, X., Becker, L.C., Becker, D.M., Starmer, J.D., Province, M.A., 2010. Avoiding the high Bonferroni penalty in genome-wide association studies. *Genet. Epidemiol.* 34, 100–105.
- 869 Ge, T., Feng, J., Hibar, D.P., Thompson, P.M., Nichols, T.E., 2012. Increasing power for voxel-wise genome-wide association studies: the random field theory, least square kernel machines and fast permutation procedures. *NeuroImage* 63, 858–873.
- 872 Grosbras, M.H., Paus, T., 2006. Brain networks involved in viewing angry hands or faces. *Cereb. Cortex* 16, 1087–1096.
- 874 Hanley, J., McNeil, B., 1982. The meaning and use of the area under a receiver operating (ROC) curve characteristic. *Radiology* 143, 29–36.
- 877 Hayasaka, S., Nichols, T.E., 2003. Validating cluster size inference: random field and permutation methods. *NeuroImage* 20, 2343–2356.
- 879 Hayasaka, S., Nichols, T.E., 2004. Combining voxel intensity and cluster extent with permutation test framework. *NeuroImage* 23, 54–63.
- 880 Hayasaka, S., Phan, K.L., Liberzon, I., Worsley, K.J., Nichols, T.E., 2004. Nonstationary cluster-size inference with random field and permutation methods. *NeuroImage* 22, 676–687.
- 883 Hibar, D.P., Stein, J.L., Kohannim, O., Jahanshad, N., Saykin, A.J., Shen, L., Kim, S., Pankratz, N., Foroud, T., Huentelman, M.J., Potkin, S.G., Jack, C.R., Weiner, M.W., Toga, A.W., Thompson, P.M., Initiative, A.D.N., 2011. Voxelwise gene-wide association study (vGeneWAS): multivariate gene-based association testing in 731 elderly subjects. *NeuroImage* 56, 1875–1891.
- 889 Holmes, A.P., Blair, R.C., Watson, J.D., Ford, I., 1996. Nonparametric analysis of statistic images from functional mapping experiments. *J. Cereb. Blood Flow Metab.* 16, 7–22.
- 891 Hutton, C., Bork, A., Josephs, O., Deichmann, R., Ashburner, J., Turner, R., 2002. Image distortion correction in fMRI: a quantitative evaluation. *NeuroImage* 16, 217–240.
- 892 Johnson, S.C., 1967. Hierarchical clustering schemes. *Psychometrika* 32, 241–254.
- 894 Keller, M., Lavielle, M., Perrot, M., Roche, A., 2009. Anatomically informed Bayesian model selection for fMRI group data analysis. *Med. Image Comput. Comput. Assist. Interv.* 12, 450–457.
- 896 Knutson, B., Westdorp, A., Kaiser, E., Hommer, D., 2000. fMRI visualization of brain activity during a monetary incentive delay task. *NeuroImage* 12, 20–27.
- 898 **Q10** Kohannim, O., Hibar, D.P., Stein, J.L., Jahanshad, N., C. R. J.J., Weiner, M.W., Toga, A.W., P.M.T., 2011. Boosting power to detect genetic associations in imaging using multi-locus, genome-wide scans and ridge regression. *Biomedical Imaging: From Nano to Macro*, 2011 IEEE International Symposium on, pp. 1855–1859.
- 902 Logan, G.D., 1994. On the ability to inhibit thought and action: a users' guide to the stop signal paradigm. *Psychol. Rev.* 91, 295–327.
- 904 Meinshausen, N., Bühlmann, P., 2010. Stability selection. *J. R. Stat. Soc. Ser. B Stat. Methodol.* 72, 417–473.
- 906 Michel, V., Gramfort, A., Varoquaux, G., Eger, E., Keribin, C., Thirion, B., 2012. A supervised clustering approach for fMRI-based inference of brain states. *Pattern Recogn.* 45, 2041–2049.
- 908 Moorhead, T.W.J., Job, D.E., Spencer, M.D., Whalley, H.C., Johnstone, E.C., Lawrie, S.M., 2005. Empirical comparison of maximal voxel and non-isotropic adjusted cluster extent results in a voxel-based morphometry study of comorbid learning disability with schizophrenia. *NeuroImage* 28, 544–552.
- 912 Nichols, T.E., Holmes, A.P., 2002. Nonparametric permutation tests for functional neuroimaging: a primer with examples. *Hum. Brain Mapp.* 15, 1–25.
- 915 Nieto-Castanon, A., Ghosh, S.S., Tourville, J.A., Guenther, F.H., 2003. Region of interest based analysis of functional imaging data. *NeuroImage* 19, 1303–1316.
- 917 Ou, W., Wells, W.M., Golland, P., 2010. Combining spatial priors and anatomical information for fMRI detection. *Med. Image Anal.* 14, 318–331.
- 919 Pedregosa, F., Varoquaux, G., Gramfort, A., Michel, V., Thirion, B., Grisel, O., et al., 2011. Scikit-learn: machine learning in Python. *J. Mach. Learn. Res.* 12, 2825–2830.
- 920 Petersson, K.M., Nichols, T.E., Poline, J.B., Holmes, A.P., 1999. Statistical limitations in functional neuroimaging. II. Signal detection and statistical inference. *Philos. Trans. R. Soc. Lond. B Biol. Sci.* 354, 1261–1281.
- 922 Poline, J.B., Mazoyer, B.M., 1993. Analysis of individual positron emission tomography activation maps by detection of high signal-to-noise-ratio pixel clusters. *J. Cereb. Blood Flow Metab.* 13, 425–437.
- 927 Poline, J.B., Worsley, K.J., Evans, A.C., Friston, K.J., 1997. Combining spatial extent and peak intensity to test for activations in functional imaging. *NeuroImage* 5, 83–96.
- 929 Puls, I., Mohr, J., Wrase, J., Vollstädt-Klein, S., Leménager, T., Vollmert, C., Rapp, M., Obermayer, K., Heinz, A., Smolka, M.N., 2009. A model comparison of comt effects on central processing of affective stimuli. *NeuroImage* 46, 683–691.
- 932 Roland, P.E., Levin, B., Kawashima, R., Åkerman, S., 1993. Three-dimensional analysis of clustered voxels in 15-o-butanol brain activation images. *Hum. Brain Mapp.* 1, 3–19.
- 934 Salimi-Khorshidi, G., Smith, S.M., Nichols, T.E., 2011. Adjusting the effect of nonstationarity in cluster-based and tfe inference. *NeuroImage* 54, 2006–2019.
- 936 Schumann, G., Loth, E., Banaschewski, T., Barbot, A., Barker, G., Bchel, C., Conrod, P.J., Dalley, J.W., Flor, H., Gallinat, J., Garavan, H., Heinz, A., Itterman, B., Lathrop, M., Mallik, C., Mann, K., Martinot, J.L., Paus, T., Poline, J.B., Robbins, T.W., Rietschel, M., Reed, L., Smolka, M., Spanagel, R., Speiser, C., Stephens, D.N., Strhle, A., Struve, M., IMAGEN consortium, 2010. The IMAGEN Study: reinforcement-related behaviour in normal brain function and psychopathology. *Mol. Psychiatry* 15, 1128–1139.
- 942 Sim, K., Chan, W.Y., Woon, P.S., Low, H.Q., Lim, L., Yang, G.L., Lee, J., Chong, S.A., Sitoh, Y.Y., Chan, Y.H., Liu, J., Tan, E.C., Williams, H., Nowinski, W.L., 2012. Arvcf genetic influences on neurocognitive and neuroanatomical intermediate phenotypes in Chinese patients with schizophrenia. *J. Clin. Psychiatry* 73, 320–326.
- 946 Smith, S.M., Nichols, T.E., 2009. Threshold-free cluster enhancement: addressing problems of smoothing, threshold dependence and localisation in cluster inference. *NeuroImage* 44, 83–98.
- 949 Smolka, M., Bühler, M., Schumann, G., Klein, S., Hu, X., Moayer, M., Zimmer, A., Wrase, J., Flor, H., Mann, K., et al., 2007. Gene-gene effects on central processing of aversive stimuli. *Mol. Psychiatry* 12, 307–317.
- 952 Sol, A.F., Ngan, S.C., Sapiro, G., Hu, X., Lpez, A., 2001. Anisotropic 2-d and 3-d averaging of fMRI signals. *IEEE Trans. Med. Imaging* 20, 86–93.
- 954 Stein, J.L., Hua, X., Lee, S., Ho, A.J., Leow, A.D., Toga, A.W., Saykin, A.J., Shen, L., Foroud, T., Pankratz, N., Huentelman, M.J., Craig, D.W., Gerber, J.D., Allen, A.N., Corneveaux, J.J., Dechairo, B.M., Potkin, S.G., Weiner, M.W., Thompson, P., Alzheimer's Disease Neuroimaging Initiative, 2010. Voxelwise genome-wide association study (vGWAS). *NeuroImage* 53, 1160–1174.
- 959 Strother, S.C., Anderson, J., Hansen, L.K., Kjems, U., Kustra, R., Sidtis, J., Frutiger, S., Muley, S., LaConte, S., Rottenberg, D., 2002. The quantitative evaluation of functional neuroimaging experiments: the npairs data analysis framework. *NeuroImage* 15, 747–771.
- 962 Thirion, B., Flandin, G., Pinel, P., Roche, A., Ciuciu, P., Poline, J.B., 2006. Dealing with the shortcomings of spatial normalization: multi-subject parcellation of fMRI datasets. *Hum. Brain Mapp.* 27, 678–693.
- 965 Thirion, B., Pinel, P., Mriaux, S., Roche, A., Dehaene, S., Poline, J.B., 2007. Analysis of a large fMRI cohort: statistical and methodological issues for group analyses. *NeuroImage* 35, 105–120.
- 968 Thyreau, B., Schwartz, Y., Thirion, B., Frouin, V., Loth, E., Vollstedt-Klein, S., Paus, T., Artiges, E., Conrod, P.J., Schumann, G., Whelan, R., Poline, J.B., Consortium I.M.A.G.E.N., 2012. Very large fMRI study using the IMAGEN database: sensitivity-specificity and population effect modeling in relation to the underlying anatomy. *NeuroImage* 61, 295–303.
- 972 Varoquaux, G., Gramfort, A., Thirion, B., 2012. Small-sample brain mapping: sparse recovery on spatially correlated designs with randomization and clustering. *Int. J. John, L., Joelle, P. (Eds.), International Conference on Machine Learning. Andrew McCallum, Edimbourg, United Kingdom.*
- 976 Ville, D.V.D., Blu, T., Unser, M., 2004. Integrated wavelet processing and spatial statistical testing of fMRI data. *NeuroImage* 23, 1472–1485.
- 978 Vounou, M., Nichols, T.E., Montana, G., Initiative, A.D.N., 2010. Discovering genetic associations with high-dimensional neuroimaging phenotypes: a sparse reduced-rank regression approach. *NeuroImage* 53, 1147–1159.
- 979 Ward, J., 1963. Hierarchical grouping to optimize an objective function. *J. Am. Stat. Assoc.* 58, 236–244.
- 983 Westfall, P.H., Troendle, J.F., 2008. Multiple testing with minimal assumptions. *Biom. J.* 50, 745–755.
- 984 Worsley, K.J., Evans, A.C., Marrett, S., Neelin, P., 1992. A three-dimensional statistical analysis for CBF activation studies in human brain. *J. Cereb. Blood Flow Metab.* 12, 900–918.
- 987 Worsley, K.J., Marrett, S., Neelin, P., Evans, A.C., 1996a. Searching scale space for activation in PET images. *Hum. Brain Mapp.* 4, 74–90.
- 989 Worsley, K.J., Marrett, S., Neelin, P., Vandal, A.C., Friston, K.J., Evans, A.C., 1996b. A unified statistical approach for determining significant signals in images of cerebral activation. *Hum. Brain Mapp.* 4, 58–73.
- 991 Wu, D.H., Lewin, J.S., Duerk, J.L., 1997. Inadequacy of motion correction algorithms in functional MRI: role of susceptibility-induced artifacts. *J. Magn. Reson. Imaging* 7, 365–370.
- 992
- 993
- 994
- 995